Journal of Power Sources 189 (2009) 1003–1007

Contents lists available at ScienceDirect

Journal of Power Sources

journal homepage: www.elsevier.com/locate/jpowsour

Synthesis of $La_{0.6}Ca_{0.4}Co_{0.8}Ir_{0.2}O_3$ perovskite for bi-functional catalysis in an alkaline electrolyte

Yun-Min Chang, Pu-Wei Wu*, Cheng-Yeou Wu, Yu-Chi Hsieh

Department of Materials Science and Engineering, National Chiao Tung University, Hsin-Chu 300, Taiwan

ARTICLE INFO

Article history:
Received 14 December 2008
Accepted 17 December 2008
Available online 30 December 2008

Keywords:
Perovskite
Bi-functional electrocatalyst
Alkaline electrolyte
Oxygen reduction
Oxygen evolution

ABSTRACT

The amorphous citrate precursor method was employed to prepare perovskite of $La_{0.6}Ca_{0.4}Co_{0.8}Ir_{0.2}O_3$ as a bi-functional electrocatalyst for oxygen reduction and evolution in an alkaline electrolyte. The X-ray diffraction pattern of the as-synthesized powders exhibited a majority phase identical to that of $La_{0.6}Ca_{0.4}CoO_3$, indicating successful incorporation of Ir^{4+} at the Co cation sites. Scanning Electron Microscope images demonstrated a foam-like microstructure with a surface area of 13.31 $m^2\,g^{-1}$. For electrochemical characterization, the $La_{0.6}Ca_{0.4}Co_{0.8}Ir_{0.2}O_3$ particles were supported on carbon nanocapsules (CNCs) and deposited on commercially available gas diffusion electrodes with a loading of 2.4 mg cm^{-2}. In current–potential polarizations, $La_{0.6}Ca_{0.4}Co_{0.8}Ir_{0.2}O_3$/CNCs revealed more enhanced bi-functional catalytic abilities than $La_{0.6}Ca_{0.4}CoO_3$/CNCs. Similar behaviors were observed in galvanostatic profiles for oxygen reduction and evolution at current densities of 50 and 100 mA cm^{-2} for 10 min. Moreover, notable changes from zeta potential measurements were recorded for $La_{0.6}Ca_{0.4}Co_{0.8}Ir_{0.2}O_3$ relative to $La_{0.6}Ca_{0.4}CoO_3$. In lifetime determinations, where a repeated 3 h sequence of oxygen reduction/resting/oxygen evolution/resting was imposed, $La_{0.6}Ca_{0.4}Co_{0.8}Ir_{0.2}O_3$/CNCs delivered a stable and sustainable behavior with moderate degradation.

1. Introduction

Oxygen molecules are abundant and reactive with most elements in forming useful compounds. Therefore, reduction and evolution of oxygen electrochemically play critical roles in many industrial devices such as batteries and fuel cells, and in the process of water electrolysis [1–3]. For example, in water electrolysis, facile oxygen evolution is desired to minimize energy consumption. In contrast, in rechargeable alkaline systems such as nickel–zinc and nickel–cadmium batteries, parasitic oxygen evolution during charging is purposely retarded for concerns in safety and coulombic efficiency [4]. On the other hand, in the operation of direct methanol and solid oxide fuel cells, rapid oxygen reduction is necessary to reduce undesirable polarization loss [5,6]. In general, electrochemical reduction and formation of oxygen require a variety of catalysts to expedite the associated reaction steps. An extensive review on oxygen electrochemistry has been provided by Kinoshita [7].

Electrocatalysts are typically designed for a single purpose only and suited for particular combinations of electrode and electrolyte. However, in systems such as rechargeable metal–air, air–metal hydrides, and regenerative fuel cells, a bi-functional electrocatalyst is warranted [8–10]. Materials with bi-functional catalytic abilities are capable of promoting oxygen reduction and evolution on the same electrode. Selection criteria for reduction electrocatalysts are relatively simple for metals, oxides, and polymers [11–13]. However, for the oxygen evolution reaction, due to the relatively high oxidative potentials involved, only a few oxides are sufficiently stable over the long term [14]. So far, perovskites (ABO_3), spinels (AB_2O_4), and pyrochlores ($A_2B_2O_7$) have been investigated with moderate success [15–17]. Among them, perovskite is considered the leading candidate because of its reasonable electrical conductivity and corrosion resistance.

In an alkaline electrolyte, perovskites of lanthanum cobaltate ($LaCoO_3$) and related compounds have received the most attention with regard to their catalytic actions [18–20]. According to Tiwari et al., the catalytic ability for oxygen reduction is attributed to the Co cation and simply by doping certain selective transition elements at the Co cation sites, the catalytic ability can be varied substantially [21]. Hence, we rationalize that the incorporation of elements designated for the catalysis of oxygen evolution at the Co cation sites could lead to enhanced bi-functional abilities. Earlier, it was reported that the oxide of IrO_2 is useful for oxygen evolution [22]. Unfortunately, concerns over possible dissolution of Ir^{4+} in an alkaline electrolyte limit this pursuit.

Due to the similarity in the atomic size and valence, we surmise that the Ir cation could occupy the Co cation site in a

* Corresponding author. Tel.: +886 3 5131227; fax: +886 3 5724727.
E-mail address: ppwu@mail.nctu.edu.tw (P.-W. Wu).

0378-7753/$ – see front matter © 2008 Elsevier B.V. All rights reserved.
doi:10.1016/j.jpowsour.2008.12.101

perovskite matrix. As a result, the perovskite structure is expected to provide necessary stability in the alkaline electrolyte, while the Ir and Co cations are responsible for catalyzing oxygen evolution and reduction, respectively. Previously, we synthesized non-stoichiometric $La_{0.6}Ca_{0.4}CoIr_{0.25}O_{3.5-\delta}$ by a mechanical alloying method and reported rather unique bifunctional catalytic behaviors [23]. However, due to the distorted perovskite lattice, the exact nature of the observed performance enhancement could not be identified. Our recent attempt to prepare stoichiometric $La_{0.6}Ca_{0.4}Co_{0.8}Ir_{0.2}O_3$ using a solid state reaction method also recorded notable catalytic improvements [24]. Nevertheless, the resulting catalytic performances were not optimized, and complete electrochemical evaluations were lacking because excess sintering led to undesirable large particles.

In this work, we synthesized powders of $La_{0.6}Ca_{0.4}Co_{0.8}Ir_{0.2}O_3$ using an amorphous citrate precursor (ACP) approach and evaluated their bi-functional catalysis in an alkaline electrolyte using carbon nanocapsules (CNCs) as the catalyst support. An identical process was performed on $La_{0.6}Ca_{0.4}CoO_3$ for comparison purposes.

2. Experimental

The amorphous citrate precursor method was adopted to prepare stoichiometric $La_{0.6}Ca_{0.4}Co_{0.8}Ir_{0.2}O_3$ perovskite in which $La(NO_3)_3{\cdot}6H_2O$, $Ca(NO_3)_2{\cdot}4H_2O$, $Co(NO_3)_3{\cdot}6H_2O$, and $IrCl_3{\cdot}xH_2O$ were dissolved at a proper ratio in excess deionized water with citric acid. The molar ratio of the citric acid to the metal ions was 1:1. The mixtures underwent moderate heating and stirring at 80 °C for 6 h to form a dry gel. Subsequently the gel was heat-treated at 650 °C for 4 h under a constant air flow to form powders.

The catalytic layer for the gas diffusion electrode (GDE) was fabricated by mixing 30 wt% $La_{0.6}Ca_{0.4}Co_{0.8}Ir_{0.2}O_3$, 30 wt% polytetrafluoroethylene (PTFE, Dupont T-30), 10 wt% poly vinyl alcohol (PVA: MW = 2000–12,000), and 30 wt% CNCs in excess deionized water to make a slurry. After mixing for 3 min, the slurry was brush-painted repeatedly onto commercially available GDEs (eVionyx Inc.) to reach a catalyst loading of 2.4 mg cm^{-2}. Next, the catalyzed GDEs were heated at 350 °C for 30 min to remove residual solvents. Lastly, they were rolled and pressed into a thickness of 300 μm.

Phase identifications of the synthesized powders were conducted by a Siemens D5000 XRD from 20° to 80° with a Cu Kα of 0.154 nm. In addition, values for surface area and density were obtained by BET (Micromeritics Tristar 3000) and a pycometer (Micromeritics AccuPyc 1340). The morphologies of the $La_{0.6}Ca_{0.4}Co_{0.8}Ir_{0.2}O_3$ particles were observed by a SEM (JEOL JSM-6700F). The zeta potential results were obtained by a NICOMO 380 ZLS.

Electrochemical characterizations were conducted with a Solartron SI1287 potentiostat for analysis in current–potential (*i*–V) polarizations, galvanostatic measurements for oxygen reduction and evolution, and lifetime determination. An area of 3 cm^2 on the backside of the GDE was exposed to ambient air during measurements. A Ti mesh coated with RuO_2/IrO_2 was used as the counter electrode, and a Zn rod (99 wt%) was selected as the reference electrode. The Zn rod was chosen because its reading indicated the operating voltage of a zinc–air cell. A 30 wt% KOH aqueous solution was used as the electrolyte. The *i*–V polarization curves were measured at a scan rate of 1 mA s^{-1}. Galvanostatic profiles were obtained for current densities of 50 and 100 mA cm^{-2} for 10 min. In the lifetime determination, the GDEs experienced repeating sequences of oxygen reduction (0.5 h), resting (1 h), oxygen evolution (0.5 h), and resting (1 h) at 25 mA cm^{-2} with a constant inflow of CO_2-filtered air. Identical procedures were conducted on the ACP-derived $La_{0.6}Ca_{0.4}CoO_3$ for comparison purposes.

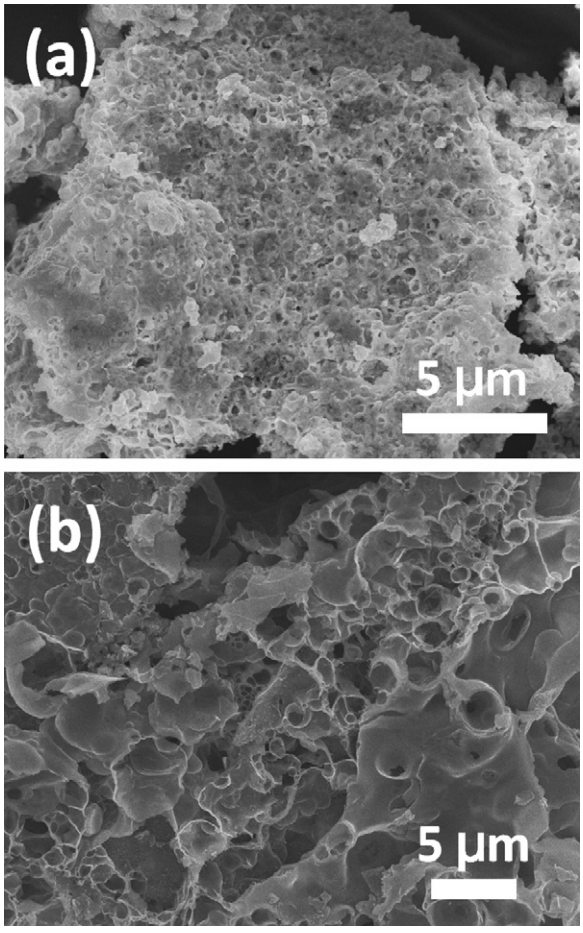

Fig. 1. SEM images for the synthesized powders of (a) $La_{0.6}Ca_{0.4}Co_{0.8}Ir_{0.2}O_3$ and (b) $La_{0.6}Ca_{0.4}CoO_3$.

3. Results and discussion

Fig. 1 presents the SEM images of the as-synthesized $La_{0.6}Ca_{0.4}Co_{0.8}Ir_{0.2}O_3$ and $La_{0.6}Ca_{0.4}CoO_3$ powders. As shown in Fig. 1(a), $La_{0.6}Ca_{0.4}Co_{0.8}Ir_{0.2}O_3$ appeared in a foam-like structure with the presence of micropores of 245 nm size. Individual particles were not discernible, and the aggregates had irregular shapes. The picture for $La_{0.6}Ca_{0.4}CoO_3$ (shown in Fig. 1(b)) reveals a similar morphology, with larger pores of 445 nm. The appearance of a foam-like microstructure is not unexpected because our sintering process was carried out under relatively mild conditions, i.e., 650 °C for 4 h. We understand that sintering at higher temperatures could produce larger particles with excessive coalescence. Measurements from the BET and pycometer on the $La_{0.6}Ca_{0.4}Co_{0.8}Ir_{0.2}O_3$ powders were 13.31 m^2 g^{-1} and 5.45 g cm^{-3}, respectively. On the other hand, the surface area and density of $La_{0.6}Ca_{0.4}CoO_3$ were 9.20 m^2 g^{-1} and 5.54 g cm^{-3}, respectively.

XRD results for the as-synthesized $La_{0.6}Ca_{0.4}Co_{0.8}Ir_{0.2}O_3$ and $La_{0.6}Ca_{0.4}CoO_3$ powders are provided in Fig. 2. As shown in Fig. 2(a), $La_{0.6}Ca_{0.4}Co_{0.8}Ir_{0.2}O_3$ exhibited a crystalline perovskite phase (ABO_3) with relevant diffraction peaks properly indexed. Unfortunately, there were minor signals possibly from the oxides of La_2O_3 ($2\theta = 36.84°$) and Co_3O_4 ($2\theta = 65.08°$). Nevertheless, we did not observe any diffraction peak from IrO_2, suggesting that the incorporation of Ir^{4+} at the Co cation sites was achieved as expected. The diffraction peaks of $La_{0.6}Ca_{0.4}Co_{0.8}Ir_{0.2}O_3$ matched nicely with those of the standard $La_{0.6}Ca_{0.4}CoO_3$ perovskite (JCPDS-36-1389). Fig. 2(b) exhibits the XRD pattern for the as-synthesized $La_{0.6}Ca_{0.4}CoO_3$, which also coincided perfectly with the standard

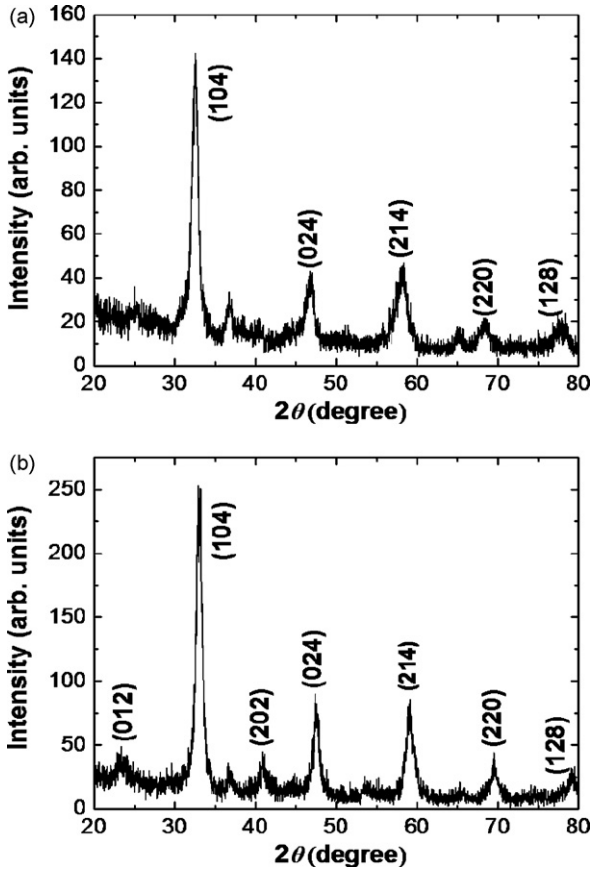

Fig. 2. X-ray diffraction patterns of the synthesized powders of (a) $La_{0.6}Ca_{0.4}Co_{0.8}Ir_{0.2}O_3$ and (b) $La_{0.6}Ca_{0.4}CoO_3$.

$La_{0.6}Ca_{0.4}CoO_3$ perovskite (JCPDS-36-1389). Similarly, we observed an extra diffraction peak at 36.90°. The simultaneous presence of these noises indicated that the undesirable phase comes from residue inherent to the ACP synthesis.

We selected the CNCs as the catalyst support because preliminary results from our evaluations indicated rather promising potentials as opposed to those of VXC72R [25]. The CNCs were produced by a flame combustion method using mixture gases of C_2H_2 and O_2 [26]. The resulting particles were considerably uniform in size and were thus favored for the GDE fabrications. Previously, Jörissen suggested that carbon supports that have excessive surface areas are prone to oxidation loss during oxygen evolution [10]. In contrast, for oxygen reduction purposes, carbon supports having large surface areas are preferred. As a result, a compromise is necessary for GDEs with bi-functional purposes. The CNCs have a moderate surface area of 333 $m^2\,g^{-1}$. Therefore, we conducted subsequent experiments using the CNCs as the catalyst support for our bi-functional studies.

Fig. 3 shows the oxygen reduction *i*–V curves for the non-catalyzed GDE and catalyzed GDEs with $La_{0.6}Ca_{0.4}Co_{0.8}Ir_{0.2}O_3$/CNCs, $La_{0.6}Ca_{0.4}CoO_3$/CNCs, and $La_{0.6}Ca_{0.4}Co_{0.8}Ir_{0.2}O_3$. Also shown is the commercial catalyst (MnO_x) from eVionyx Inc. The profiles exhibited typical *i*–V polarizations in which the potential values decreased steadily from 1.60 V with increasing current densities. Among these samples, $La_{0.6}Ca_{0.4}Co_{0.8}Ir_{0.2}O_3$/CNCs demonstrated the highest performance, delivering 1.047 and 0.932 V at 100 and 200 mA cm^{-2}, respectively. In contrast, $La_{0.6}Ca_{0.4}CoO_3$/CNCs maintained a potential of 0.891 and 0.723 V at identical current densities. There was a substantial 209 mV enhancement at 200 mA cm^{-2} for $La_{0.6}Ca_{0.4}Co_{0.8}Ir_{0.2}O_3$/CNCs. Moreover, $La_{0.6}Ca_{0.4}Co_{0.8}Ir_{0.2}O_3$/CNCs performed better than

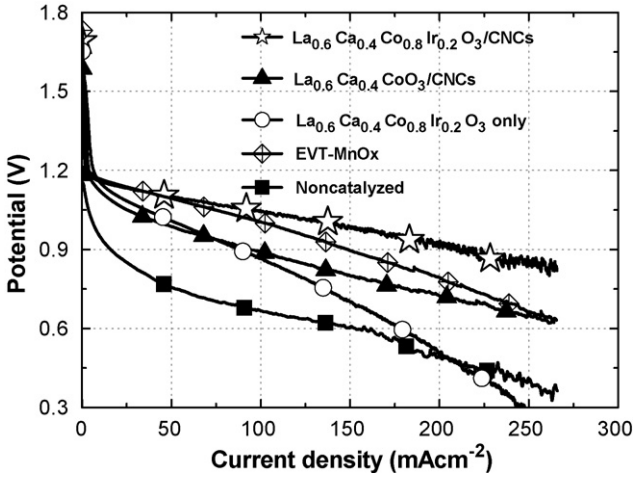

Fig. 3. Oxygen reduction *i*–V polarization curves of MnO_x, non-catalyzed GDE, and catalyzed GDEs with $La_{0.6}Ca_{0.4}Co_{0.8}Ir_{0.2}O_3$/CNCs, $La_{0.6}Ca_{0.4}CoO_3$/CNCs, and $La_{0.6}Ca_{0.4}Co_{0.8}Ir_{0.2}O_3$.

MnO_x. In contrast, the GDE with unsupported $La_{0.6}Ca_{0.4}Co_{0.8}Ir_{0.2}O_3$ demonstrated rapid voltage deterioration with increasing current densities. This behavior is consistent with earlier observations in which a synergistic effect was observed for GDEs catalyzed by perovskites supported on carbons [7]. Lastly, the non-catalyzed GDE showed negligible catalytic behaviors, as expected.

The oxygen evolution *i*–V curves for the non-catalyzed GDE, as well as GDEs catalyzed by $La_{0.6}Ca_{0.4}Co_{0.8}Ir_{0.2}O_3$/CNCs, $La_{0.6}Ca_{0.4}CoO_3$/CNCs, and IrO_2/CNCs are provided in Fig. 4. Since the oxygen evolution is kinetically challenging, the polarization loss is expected to be more severe as compared to the oxygen reduction at identical current densities. As shown, the voltage started at 1.60 V and moved rapidly to higher values with increasing current densities. Apparently, the non-catalyzed GDE showed limited oxygen evolution performance. In contrast, the GDE catalyzed by $La_{0.6}Ca_{0.4}Co_{0.8}Ir_{0.2}O_3$/CNCs demonstrated remarkable catalytic abilities, exhibiting voltages of 2.046 and 2.178 V at 50 and 100 mA cm^{-2}, respectively. At identical current densities, the voltage readings from $La_{0.6}Ca_{0.4}CoO_3$/CNCs were 2.171 and 2.347 V, respectively. The GDE catalyzed by IrO_2/CNCs showed slightly better behavior than $La_{0.6}Ca_{0.4}CoO_3$/CNCs but was still outperformed by $La_{0.6}Ca_{0.4}Co_{0.8}Ir_{0.2}O_3$/CNCs. The results from the *i*–V measurements for oxygen reduction and evolution were encouraging. With

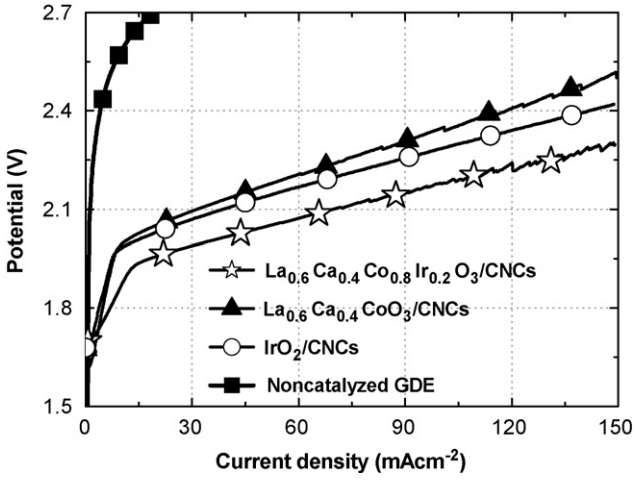

Fig. 4. Oxygen evolution *i*–V polarization curves of non-catalyzed GDE and catalyzed GDEs with $La_{0.6}Ca_{0.4}Co_{0.8}Ir_{0.2}O_3$/CNCs, $La_{0.6}Ca_{0.4}CoO_3$/CNCs, and IrO_2/CNCs.

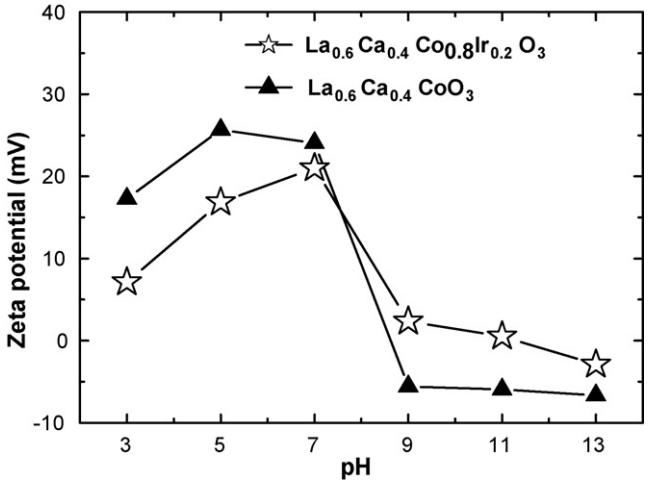

Fig. 5. Zeta potential responses for $La_{0.6}Ca_{0.4}Co_{0.8}Ir_{0.2}O_3$ and $La_{0.6}Ca_{0.4}CoO_3$.

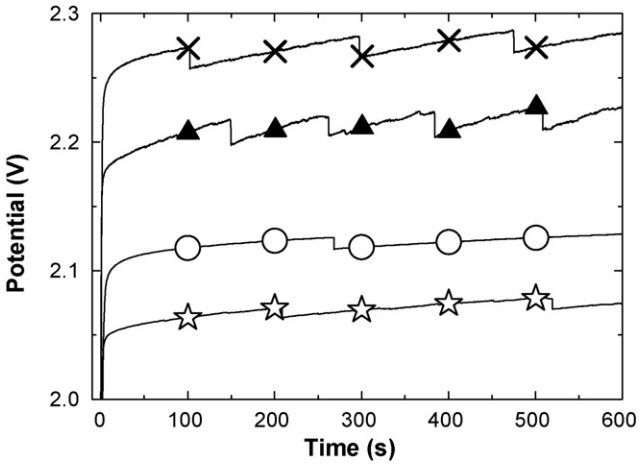

Fig. 7. Oxygen evolution galvanostatic curves for $La_{0.6}Ca_{0.4}Co_{0.8}Ir_{0.2}O_3$/CNCs at current densities of 50 mA cm^{-2} (☆) and 100 mA cm^{-2} (○), as well as $La_{0.6}Ca_{0.4}CoO_3$/CNCs at current densities of 50 mA cm^{-2} (▲) and 100 mA cm^{-2} (×).

the introduction of Ir at the Co cation sites, we not only observed improvements in the catalysis for the oxygen evolution but also unexpectedly acquired better oxygen reduction behaviors.

Additional supporting evidence could be provided by the measurement of zeta potentials. As pointed out by Bockris and Otagawa, the point of zero charge (pzc) is an indicator of intrinsic catalytic properties because the surface characteristics of oxide powders determine their pzc values [27]. Hence, the zeta potential measurements were conducted on $La_{0.6}Ca_{0.4}Co_{0.8}Ir_{0.2}O_3$ and $La_{0.6}Ca_{0.4}CoO_3$ with the results exhibited in Fig. 5. As shown, the pzc values for $La_{0.6}Ca_{0.4}Co_{0.8}Ir_{0.2}O_3$ and $La_{0.6}Ca_{0.4}CoO_3$ were determined to be 11.23 and 8.652, respectively. Our results were consistent with what Bockris and Otagawa had predicted: that the perovskites with pzc at high pH values were likely to reveal better catalytic abilities for the oxygen evolution reaction [27].

Galvanostatic measurements for the oxygen reduction reaction were carried out at current densities of 50 and 100 mA cm^{-2} for the GDEs catalyzed with $La_{0.6}Ca_{0.4}Co_{0.8}Ir_{0.2}O_3$/CNCs and $La_{0.6}Ca_{0.4}CoO_3$/CNCs. Fig. 6 demonstrates their respective profiles for 10 min. For both samples, the voltage plateaus were flat and their values agreed well with those reported in earlier *i*–V polarization curves (shown in Fig. 3), indicating that the catalytic performances of $La_{0.6}Ca_{0.4}Co_{0.8}Ir_{0.2}O_3$/CNCs and $La_{0.6}Ca_{0.4}CoO_3$/CNCs were stable and sustainable. In addition, the voltage readings from $La_{0.6}Ca_{0.4}Co_{0.8}Ir_{0.2}O_3$/CNCs were consistently higher than those of $La_{0.6}Ca_{0.4}CoO_3$/CNCs for both current densities. Fig. 7 presents the oxygen evolution galvanostatic profiles for the GDEs catalyzed with $La_{0.6}Ca_{0.4}Co_{0.8}Ir_{0.2}O_3$/CNCs and $La_{0.6}Ca_{0.4}CoO_3$/CNCs at current densities of 50 and 100 mA cm^{-2} for 10 min. Again, the voltage readings agreed nicely with earlier *i*–V polarization curves (shown in Fig. 4), and their responses were relatively steady.

Notably, $La_{0.6}Ca_{0.4}Co_{0.8}Ir_{0.2}O_3$/CNCs behaved much better than $La_{0.6}Ca_{0.4}CoO_3$/CNCs for both current densities. Unfortunately, at a current density of 100 mA cm^{-2}, severe voltage fluctuations were taking place for both samples. This is not unusual since for the oxygen evolution reaction formation and detachment of oxygen bubbles at the electrode surface often resulted in the reactivation of catalytic surfaces [28,29]. As a result, a periodic reduction of overpotentials was observed.

To fairly evaluate the bi-functional abilities of $La_{0.6}Ca_{0.4}Co_{0.8}Ir_{0.2}O_3$/CNCs, the catalyzed GDE was subjected to repeated sequences of oxygen reduction (0.5 h), resting (1 h), oxygen evolution (0.5 h), and resting (1 h) for intermittent life time determinations. Each cycle lasted 3 h, and the average voltage in respective oxygen reduction and evolution steps was measured. The results are shown in Fig. 8. For the oxygen evolution reactions, the voltages drifted lower initially but moved up steadily at a rate of

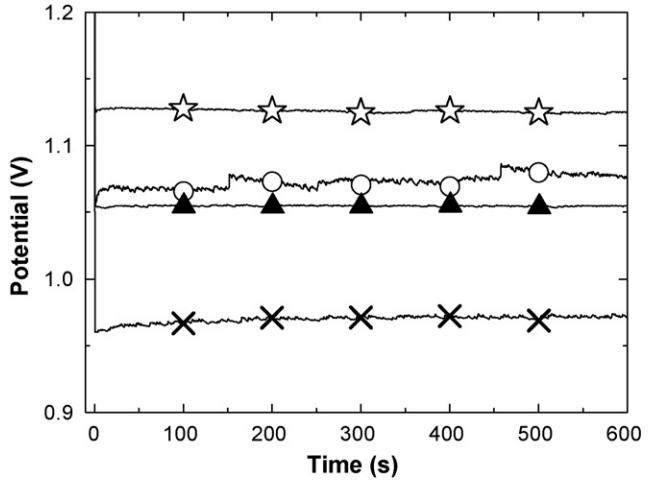

Fig. 6. Oxygen reduction galvanostatic curves for $La_{0.6}Ca_{0.4}Co_{0.8}Ir_{0.2}O_3$/CNCs at current densities of 50 mA cm^{-2} (☆) and 100 mA cm^{-2} (○), as well as $La_{0.6}Ca_{0.4}CoO_3$/CNCs at current densities of 50 mA cm^{-2} (▲) and 100 mA cm^{-2} (×).

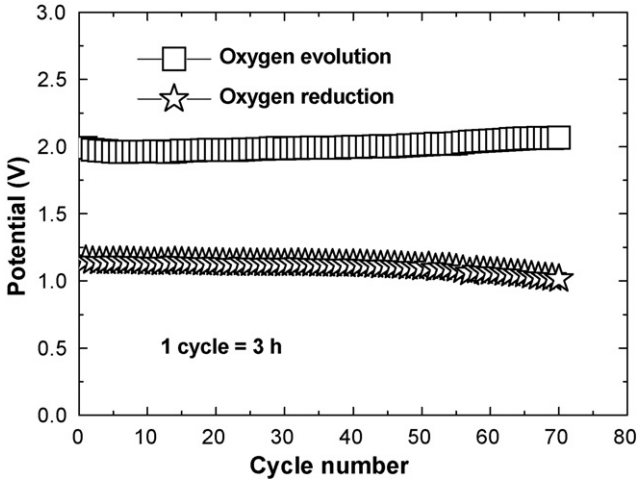

Fig. 8. The cycle life performance of $La_{0.6}Ca_{0.4}Co_{0.8}Ir_{0.2}O_3$/CNCs-catalyzed GDE.

1.59 mV cycle^{-1}. At the 70th cycle, the voltage was 2.08 V. Similarly, the voltages in the oxygen reduction reactions exhibited a gradual reduction upon cycling. The slopes of the voltage declines were 0.61 mV cycle^{-1} in the first stage (0–40 cycles) and 4.24 mV cycle^{-1} in the second stage (40–70 cycles). At the 70th cycle, the voltage was still 0.97 V. Since CO_2-filtered air was used, the effect of carbonation-induced electrode damage could be ruled out. We suspect that the undesirable electrolyte flooding contributed partially to the observed performance degradations because in our case only a thin layer of catalysts was deposited on the surface of the GDEs. In addition, it is recognized that oxidation of the carbon supports during the oxygen evolution reaction might have led to the gradual loss of catalytic abilities [30,31].

4. Conclusions

The perovskite of $La_{0.6}Ca_{0.4}Co_{0.8}Ir_{0.2}O_3$ was prepared by using an amorphous citrate precursor method. XRD analysis on the synthesized powders confirmed the majority phase to be $La_{0.6}Ca_{0.4}CoO_3$, indicating successful incorporation of Ir^{4+} at the Co cation sites. SEM images revealed a foam-like microstructure with numerous sub-micron pores. In *i*–V polarizations, $La_{0.6}Ca_{0.4}Co_{0.8}Ir_{0.2}O_3$/CNCs exhibited more enhanced bi-functional catalytic abilities than $La_{0.6}Ca_{0.4}CoO_3$/CNCs. Similar behaviors were observed by galvanostatic measurements for oxygen reduction and evolution reactions. In lifetime determinations, where repeated cycling of oxygen reduction/resting/oxygen evolution/resting was imposed, $La_{0.6}Ca_{0.4}Co_{0.8}Ir_{0.2}O_3$/CNCs demonstrated stable and sustainable performances with moderate degradation. Our results provided conclusive evidence that the doping of Ir in the perovskite structure of $La_{0.6}Ca_{0.4}CoO_3$ significantly enhances its bi-functional abilities in the alkaline electrolyte.

Acknowledgements

Financial support (T5469510026) from the Taiwan Power Company is noted. Appreciation is extended to Professor George Tu and Professor Pang Lin for an equipment loan. Carbon nanocapsules were kindly provided by Professor Yuan-Yao Li of National Chung Cheng University.

References

[1] D. Linden, T.B. Reddy, Handbook of Batteries, third ed., McGraw-Hill, New York, 2002, pp. 38.1–38.53.
[2] X. Zhou, B. Hu, Z. Chen, F. Delgado, R. Srivastava, Electrochem. Solid-State Lett. 8 (2005) A616–A618.
[3] H. Michishita, Y. Misumi, D. Haruta, T. Masaki, N. Yamamoto, H. Matsumoto, T. Ishihara, J. Electrochem. Soc. 155 (2008) B969–B971.
[4] D.C.R. Espinosa, J.A.S. Tenório, J. Power Sources 157 (2006) 600–604.
[5] C. Jeyabharathi, P. Venkateshkumar, J. Mathiyarasu, K.L.N. Phani, Electrochim. Acta 54 (2008) 448–454.
[6] X.J. Chen, K.A. Khor, S.H. Chan, J. Power Sources 123 (2003) 17–25.
[7] K. Kinoshita, Electrochemical Oxygen Technology, John Wiley & Sons Inc, New York, 1992, pp. 168–176.
[8] X. Wang, P.J. Sebastian, M.A. Smit, H. Yang, S.A. Gamboa, J. Power Sources 124 (2003) 278–284.
[9] D. Chartouni, N. Kuriyama, T. Kiyobayashi, J. Chen, J. Alloys Compd. 330–332 (2002) 766–770.
[10] L. Jörissen, J. Power Sources 155 (2006) 23–32.
[11] C.W.B. Bezerra, L. Zhang, H. Liu, K. Lee, A.L.B. Marques, E.P. Marques, H. Wang, J. Zhang, J. Power Sources 173 (2007) 891–908.
[12] N. Yoshinaga, W. Sugimoto, Y. Takasu, Electrochim. Acta 54 (2008) 566–573.
[13] S. Pylypenko, S. Mukherjee, T.S. Olson, P. Atanassov, Electrochim. Acta 53 (2008) 7875–7883.
[14] J. Lipkowski, P.N. Ross, Electrochemistry of Novel Materials, VCH Publishers, New York, 1994, 207-295.
[15] K. Watanabe, M. Yuasa, T. Kida, K. Shimanoe, Y. Teraoka, N. Yamazoe, Solid State Ionics 179 (2008) 1377–1381.
[16] M. El Baydi, S.K. Tiwari, R.N. Singh, J.L. Rehspringer, P. Chartier, J.F. Koening, G. Poillerat, J. Solid State Chem. 116 (1995) 157–169.
[17] A. Widelöv, N.M. Markovic, P.N. Ross, J. Electrochem. Soc. 143 (1996) 3504–3511.
[18] N.L. Wu, W.R. Liu, S.J. Su, Electrochim. Acta 48 (2003) 1567–1571.
[19] M. Bursell, M. Pirjamali, Y. Kiros, Electrochim. Acta 47 (2002) 1651–1660.
[20] R.N. Singh, B. Lal, Int. J. Hydrogen Energy 27 (2002) 45–55.
[21] S.K. Tiwari, S.P. Singh, R.N. Singh, J. Electrochem. Soc. 143 (1996) 1505–1510.
[22] C.P. De Pauli, S. Trasatti, J. Electroanal. Chem. 538–539 (2002) 145–151.
[23] Y.M. Chang, P.W. Wu, C.Y. Wu, Y.F. Hsieh, J.Y. Chen, Electrochem. Solid-State Lett. 11 (2008) B47–B50.
[24] Y.M. Chang, Y.C. Hsieh, P.W. Wu, C.H. Lai, T.Y. Chang, Mater. Lett. 62 (2008) 4220–4222.
[25] Y.M. Chang, Y.C. Hsieh, P.W. Wu, Diamond Relat. Mater. 18 (2009) 501–504.
[26] T.C. Liu, Y.Y. Li, Carbon 44 (2006) 2045–2050.
[27] J.O'M. Bockris, T. Otagawa, J. Electrochem. Soc. 131 (1984) 290–302.
[28] D. Kiuchi, H. Matsushima, Y. Fukunaka, K. Kuribayashi, J. Electrochem. Soc. 153 (2006) E138–E143.
[29] T. Iida, H. Matsushima, Y. Fukunaka, J. Electrochem. Soc. 154 (2007) E112–E115.
[30] N. Staud, P.N. Ross, J. Electrochem. Soc. 133 (1986) 1079–1084.
[31] P.N. Ross, M. Sattler, J. Electrochem. Soc. 135 (1988) 1464–1470.